International Journal of Concrete Structures and Materials

RESEARCH Open Access

Numerical and Experimental Analysis to Develop a SB6/H3 High Containment Level Concrete Median Barrier

Yoseok Jeong[1], Ilkeun Lee[2], Jaeha Lee[3], Kyeongjin Kim[3], Geunhyeong Min[4] and WooSeok Kim[4*]

Abstract

As the number of heavy vehicles on the road continues to increase, collisions involving heavy vehicles and concrete median barriers (CMB) occur more frequently than in the past. Consequently, there is a growing need for research into more stringent design standards and improvements to the current CMB and their performance under harsh conditions. High-performance CMB is required to in order to withstand such conditions. This paper presents the results of numerical simulations and full-scale field tests to develop a high-performance CMB. To facilitate the development of the high-performance CMB, the concept of a deformable CMB was applied to the rigid CMB. A new apparatus called the shock absorber composed of dowel bars surrounded by empty space were introduced to make the rigid CMB deformable. In order to prevent local failure at the top of the barrier from a sudden high increase in impact energy, the deformable CMB was strengthened by adding reinforcements and widening the top based on the results of numerical simulations. The full-scale field tests were conducted on the proposed deformable CMB and took into account three appraisal areas: (1) structural adequacy, (2) occupant risk, and (3) vehicle trajectory after collision. The results of these tests showed that the deformable CMB contained and redirected the vehicle without allowing it to penetrate or override the deformable CMB. No detached elements, fragmentation, or other debris from the barrier were present. Therefore, the proposed high-performance CMB fulfilled all of the requirements of the crash test guideline.

Keywords High-performance concrete median barrier, Deformable concrete median barrier, Vehicular impact simulation, Full-scale field test

1 Introduction

Safety is one of the most important aspects of road traffic. The automotive industry is constantly developing new vehicle safety systems to increase the safety of vehicle occupants. Road safety has also been improved by installing more effective roadside and median area safety systems. In many countries, the median barriers that are designed according to their guidelines (AASHTO, 2016; CEN, 2012; JRA, 2008; MOLIT, 2015) provide certain levels of vehicle containment, redirecting errant vehicles back onto the road. The number of vehicles using expressways has gradually increased, and the number of heavy vehicles alone has increased by 19% in less than 5 years in South Korea (Kim et al., 2018). There is

Journal information: ISSN 1976-0485 / eISSN 2234-1315

*Correspondence:
WooSeok Kim
wooseok@cnu.ac.kr
[1] Department of Construction and Disaster Prevention Engineering, Kyungpook National University, Gyeongbuk 37224, Republic of Korea
[2] Construction & Environment Research Group, Expressway & Transportation Research Institute, 922 Dongbudae-ro, Hwaseong, Gyeonggi-do 20896, Republic of Korea
[3] Department of Civil Engineering, Korea Maritime and Ocean University, 727 Taejong-ro, Youngdo-gu, Busan 49112, Republic of Korea
[4] Department of Civil Engineering, Chungnam National University, 99 Daehak-ro, Yuseong-gu, Daejeon 34134, Republic of Korea

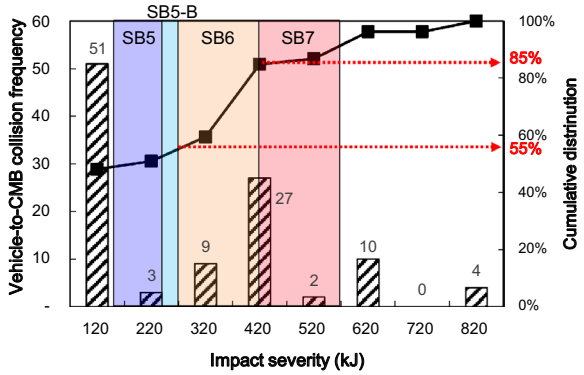

Fig. 1 Vehicle-to-CMB collision frequency versus IS calculated based on crash reports and records

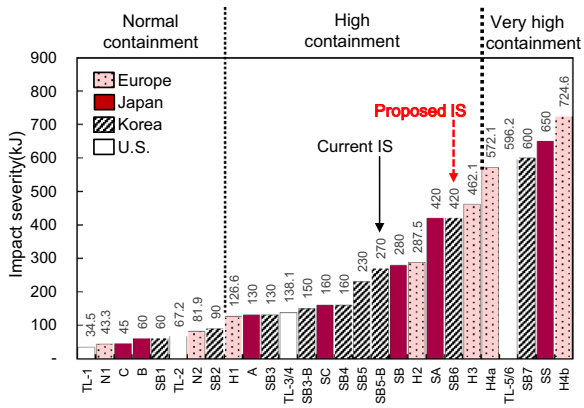

Fig. 2 Comparison of proposed IS with other countries (AASHTO, 2016; CEN, 2012; JRA, 2008; MOLIT, 2015)

a pressing need to improve the current concrete median barrier (CMB), CMB-15, which was designed for containment level SB5-B (impact severity (IS) of 270 kJ) (MOLIT, 2015). Fig 1 shows the number of vehicle–CMB collision accidents by level of impact severity based on crash reports and records in South Korea past six years. Based on this data, 45% of the total collision accidents exceed the current target impact capacity of CMB-15. If the containment level of the current CMB was upgraded to a level SB6 (IS = 420 kJ), it would be able to resist the impact severity of 85% of all accidents with no severe damage to the CMB. In the present study, a high-performance CMB is required to have a high containment level, such as SB6, which is equivalent to IS = 420 kJ, as shown in Fig. 1. The SB6 grade is designed to withstand a vehicle mass of 25,000 kg, vehicle speed of 80 km/h, and impact of angle 20°(MOLIT, 2015). This standard is similar to an SA grade of 420 kJ (Japan) and an H3 grade of 462.1 kJ (Europe), as shown in Fig. 2. Containment level SB6 can handle 1.55 times more impact severity than the current standard SB5-B.

Safety barriers generally fall into two categories: flexible and rigid (Ferdous et al., 2011). A flexible barrier is normally made of steel or aluminum, absorbing a large portion of the kinetic energy of a colliding vehicle and resulting in irreversible deformation. This may effectively reduce the energy shift to the interior of the vehicle, and therefore save the driver from fatal injury (Ferdous et al., 2011). A concrete barrier is a typical rigid barrier which is usually placed in the roadway where two-way traffic is close to prevent vehicle crossover during collisions in accident-prone regions with high traffic volumes and speeds. The kinetic energy of the moving vehicle transfers primarily to the internal energy of the vehicle itself and very little to the barrier. Therefore, the vehicle may be seriously damaged and its occupants are often seriously injured (Naish & Burbridge, 2015). When the containment level of a concrete barrier is increased and a heavy vehicle collides at high speed with the barrier, the chance of severe collapse of the vehicle and injury to the driver also increases. However, the concept of a deformable concrete barrier has been applied to the design of a high containment-level concrete barrier so that the final product would better absorb and dissipate the kinetic energy from a colliding vehicle by giving way to its own deformation.

Kim et al. (2018) were the first to introduce a deformable CMB. Empty chambers inside the barrier were shaped by packing Styrofoam around each dowel bar, making space for the bars to bend on impact (Fig. 3). The lateral bending of the concrete and dowel bars could absorb the impact energy. Fig. 3 shows the lateral displacement and resistance length. Lateral displacement indicates the amount of deformation that is normal to the longitudinal direction, whereas the resistance length is the longitudinal length in which the lateral displacement occurs owing to impact with respect to the longitudinal axis of the CMB. As Fig. 3 shows, the undeformable CMB (CMB-15) response includes localized plastic deformation (represented by the red region in Fig. 3), which can produce a large amount of concrete fragments, resulting in collateral damage to vehicles in the opposite lane. By contrast, the deformable CMB benefits not only from deforming the dowel bar by absorbing impact energy but also disperses deformations within the resistance length, which dissipates the impact energy over a much larger area of the CMB. The results of numerical analysis in a sensitivity study by Kim et al. (2018) and Kim et al. (2019) showed that a deformable CMB with empty internal chambers absorbed significant collision energy. The performance of the deformable CMB with regard to impact energy dissipation was also verified by full-scale field test data (Lee et al., 2017, 2019).

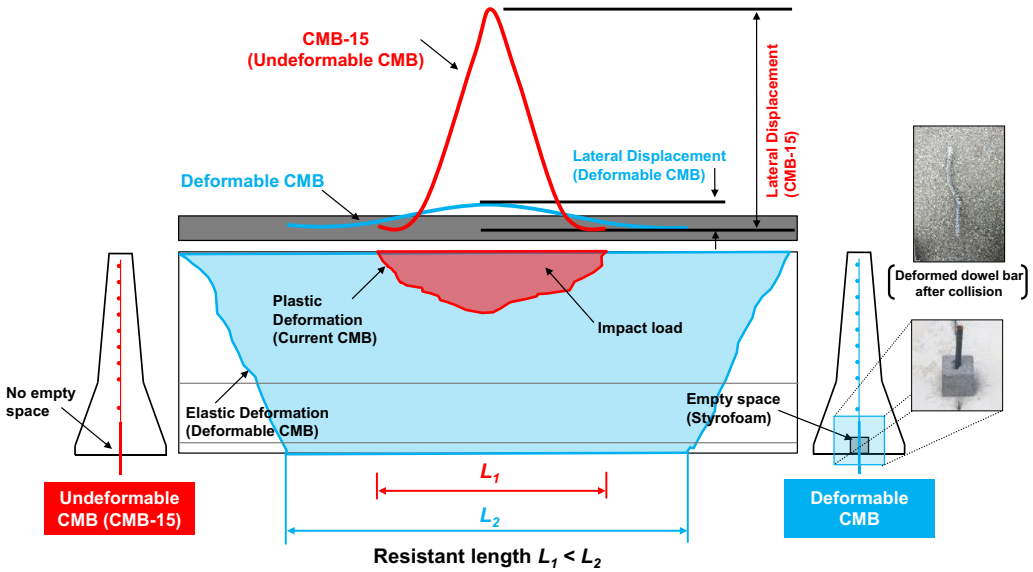

Fig. 3 Advantage of deformable concrete median barrier (CMB) compared with the CMB-15, which limits lateral displacement in a vehicle-to-barrier collision

Since the currently installed CMBs (CMB-15, as shown in Fig. 4(a)) were designed to have a containment level of SB5-B/H2 (SB6 and H3 are grade of Impact Severity, 270 kJ for Korea and Europe, respectively; see Fig. 2), they are consequently vulnerable at higher containment levels such as SB6/H3 (SB6 and H3 are grade of impact severity, 420 kJ for Korea and Europe, respectively.). Deformable CMBs designed with empty space around each dowel bar were introduced not only to prevent secondary accidents to vehicles in the oncoming traffic from concrete fragments, but also to accommodate high containment-level collisions such as SB6/H3. The first deformable CMB configurations featured top barrier widths of 200 mm, two layers of D7.6 (100 mm × 100 mm wire mesh), and a novel shock absorber comprising D19 dowel bars and cubic Styrofoam. The first deformable CMB called as CMB-16 showed enough structural integrity and deformation under SB5-B (20A) (IS = 456 kJ), or vehicle of 14,000 kg, speed of 85 km/h, and impact angle of 20° (Kim et al., 2018; Lee et al., 2017). More details regarding a parametric study and full-scale field testing about the deformable CMB are in the journal *Journal of Performance of Constructed Facilities* (Kim et al., 2018). The objective of this research is to propose a novel deformable CMB with a containment level of SB6/H3 that complies with the current test guidelines. To this end, a parametric study and full-scale field tests were conducted.

2 Development of a Deformable Concrete Median Barrier, CMB-17S

2.1 Numerical Model for Vehicle-to-Barrier Collision

Several computer simulations of vehicle-to-barrier were carried out in the last few years by means of numerical simulation software tools as MADYMO (Grzebieta et al., 1999) or LS-DYNA (Ahn et al., 2021; Borovinšek et al., 2007; Dinnella et al., 2020; Ferdous et al., 2013; Yin et al., 2016). In this research, numerical simulations were employed to develop a deformable concrete median barrier. The analyses were conducted by using finite element

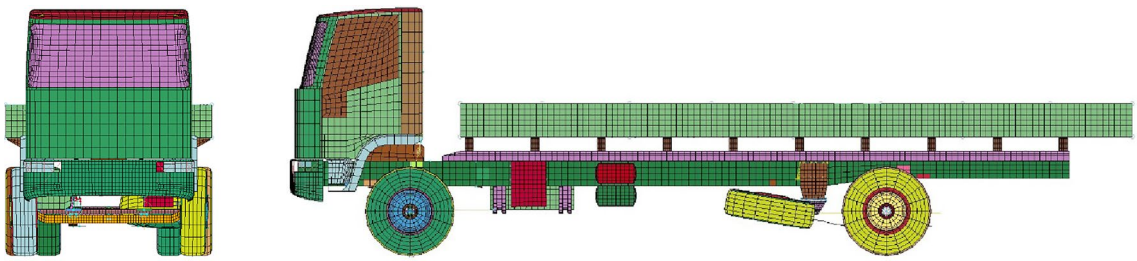

Fig. 4 NCAC (National Crash Analysis Center) truck model used for crash simulation of vehicle-to-barrier collisions (NCAC, 2020)

code LS-DYNA (LSTC, 2007) that is a well-known software for performing vehicular crash test simulations.

2.1.1 Vehicle Model

The finite element (FE) vehicle model for vehicle-to-barrier collisions was developed by the National Crash Analysis Center (NCAC) based on European Standard EN 1317 (CEN, 2012), as shown in Fig. 4. The dimensions of the selected models were similar to those of Korean trucks and were therefore appropriate for numerical simulation of vehicle-to-barrier collisions.

2.1.2 Concrete Model

The LS-DYNA software provides several constitutive models of concrete for impact loading. The behavior of a concrete barrier under impact loads is composed of local deformation in the proximity of the vehicle-to-barrier contact within a very short time and the overall deformation of the whole barrier over a relatively long time. Numerical simulation of these deformations requires an appropriate concrete material model capable of capturing typical concrete material behavior under a general stress state. There are several concrete constitutive models available to simulate impact loads. Three of the widely available models are Winfrith (MATFh84-085), KCC (MAT_072R3), and continuous surface cap model (CSCM) (MAT_159). Although the Winfrith model can predict crack initiation/propagation and allow crack visualization, deformation could be underestimated when compared with the KCC and CSCM models owing to the absence of post-peak softening in compression (Chung et al., 2011). On the other hand, the KCC and CSCM models include a parameter-generation capability and can simulate typical concrete material behavior, such as post-peak softening in compression and tension, strain rate effect, and shear dilation, which are suitable for quasi-static, blast, and impact loads (Madurapperuma & Niwa, 2014; Wu et al., 2012). The CSCM model has shown an excellent capability to simulate vehicle-to-structure collisions (Auyeung et al., 2019; Kim et al., 2018, 2019; Lee et al., 2017, 2019; Saini & Shafei, 2018, 2019). Accordingly, the CSCM model was used for a concrete constitutive model for the vehicle-to-barrier collision in this study, taking into consideration the structure type, automatic parameter generation, and availability of material properties.

In CSCM model, when the strain energy exceeds a predetermined threshold, damage starts to occur and accumulate throughout the duration of the simulation. An element erodes owing to damage accumulation according to a user-defined input value such as "ERODE" (Murray, 2007), which is very useful for quantifying the structural damage caused by impact loads. In the CSCM model, ERODE was introduced to simulate the cracking of concrete. ERODE is a plastic deformation rate which defines the deletion of elements after the energy inside the element is exhausted due to collision. The values of ERODE used by past researchers are 1.0 (Murray, 2007), and 1.4 (El-Tawil et al., 2005). In the present study, we selected 1.2 as the value of ERODE because for this value the configurations of cracks and breakage after collision were similar to the results of actual collision tests. The strain rate effect was considered by activating the IRATE option. The rate effect of impact loads on structural behavior is modeled using the "REPOW", which increases the fracture energy of the concrete (Murray, 2007). The REPOW parameter is used to modulate the strain rate effect in simulations of material deformation and fracture as follows:

$$G_f^{vp} = G_f \left[1 + \frac{E\dot{\epsilon}\eta}{r^5\sqrt{E}}\right]^{REPOW}. \quad (1)$$

The key parameters involved in this equation are: REPOW, which increases fracture energy with rate effects; scaled up rate effects value(G_f^{vp}); fracture energy (G_f); damage threshold before viscoplasticity (r); elastic modulus (E); effective strain rate ($\dot{\epsilon}$); and rate effects parameter (η). In this study, we selected a REPOW value of 3 based on the findings of Kim et al. (2018) and Lee et al. (2019), who demonstrated that this value produced damage configurations that closely matched those observed in actual collisions. Therefore, we used a REPOW value of 3 in our simulations to accurately model the physical phenomena of interest. In this study, user input parameters are used for the CSCM model based on results by Kim et al. (2018) and Lee et al. (2019) including the strain rate effect and appropriate material erosion criteria. The CSCM model with automatic parameter generation requires an unconfined compressive strength and maximum aggregate size as inputs. In the numerical simulation, the unconfined compressive strength of concrete was 30 MPa and its maximum aggregate size was 20 mm. The prediction equation for the fracture energy in the CSCM model is calculated based on the CEB-FIP model code (1990). This equation predicts relatively smaller fracture energies and differs from the recent equations. Thus, the most recent CEB-FIP model code (2012) was used for calculations in this study. The concrete tensile strength and fracture energy were estimated based on the compressive strength and aggregate size using the design standard (CEB-FIP, 2012):

$$f_t = 0.3\left(f_{ck}\right)^{2/3}, \quad (2)$$

$$G_F = 73\left(f_{cm}\right)^{0.18}. \quad (3)$$

Here, f_t is the tensile strength (MPa), f_{ck} is the characteristic compressive strength (MPa), f_{cm} is the mean compressive strength, and G_F is the fracture energy (N/m). In CSCM model, three types of fracture energy are defined: compressive, tensile, and shear. The same values were used for the tensile and shear fracture energies, as they both represent the resistance of the material to crack propagation. However, the compressive fracture energy was set to be 100 times greater than the tensile fracture energy. In this study, the fracture energy values were determined using a prediction equation based on CEB-FIP to ensure accuracy and consistency with industry standards.

2.1.3 Contact Model at Vehicle-to-Barrier Collision

The automatic_single_surface option was used to model the contact between the vehicle and the CMB. This option automatically calculates the contact between the selected parts, which is why it was selected. It is difficult to predict which part of the vehicle will come into contact with the median barrier during the analysis, hence the use of this option. Therefore, this option is especially helpful when there are a large number of parts in a body and the position of the contact formation is not known in the model. In the selected contact algorithms, the coefficients for dynamic and static friction were assumed to be 0.08 and 0.05, respectively, as recommended in the literature (Chung et al., 2011).

2.1.4 LS-DYNA Parameters for Vehicle-to-Barrier Collision

In this study, the LS-DYNA parameters were selected for a vehicle-to-barrier collision simulation, as shown in Table 1. Lee et al. (2017) investigated the influence of ERODE and REPOW on the local and global behaviors of a CMB under vehicle impact. The numerical results from using the CSCM model were found to be very sensitive to the values of ERODE and REPOW, which could lead to stability issues (Kim et al., 2018; Lee et al., 2017). Therefore, recommended values were used in the CSCM model based on the numerical results of a parametric study compared with full-scale field tests of a vehicle-to-barrier collision (Kim et al., 2018; Lee et al., 2017, 2019).

Table 1 LS-DYNA parameters used for vehicle-to-barrier collision (Chung et al., 2011; Kim et al., 2018, 2019; Lee et al., 2017, 2019)

Parameter	Value
ERODE	1.2
REPOW	3.0
Hourglass control	0.03
Vehicle-to-barrier friction coefficient (dynamic/static)	0.8/0.5

Hourglass control was also considered to minimize the hourglass energy. Among several options considered, Flanagan–Belytschko (stiffness formulation) was found to be suitable for this model.

2.2 Results of Parametric Study for Development of the CMB-17S

In this section, numerical results from developed FE models are presented to propose the CMB-17S with a containment level of SB6/H3 (IS = 420 kJ). The key parameters, 100 mm × 100 mm diameter size of the wire mesh and dowel bars for shock absorbers, were considered in this parametric study, and the results are shown in Fig. 5. It should be noted that the volume loss ratio used in Fig. 5 was calculated by dividing the weight of the eroded concrete elements from the simulations by the total weight of a meter-long section of CMB. An allowable volume loss ratio of 3.5% was selected for the design purposes of the CMB-17S. In a full-scale field test of CMB-15, the volume loss ratio was 7.0%volume loss ratio, and this met all the requirements of the test guidelines (Lee et al., 2017). An allowable volume loss ratio of 3.5% is conservative for designing the new deformable CMB. Fig 5 shows the volume loss ratio in a bar chart format, in terms of dowel bar size and wire diameter (100 mm × 100 mm). In general, a smaller the volume loss ratio can be correlated with increases in the sizes of dowel bars and wire. Although the volume loss ratio appears lower than allowable for several cases of 3.5- and 4.5 mm wire mesh, the D25 dowel bars show significantly high volume loss. This is attributable to the high stiffness of the 25-mm dowel bar. A thicker dowel bar is less likely to deform under an impact load. Considering the impact energy dissipation caused by dowel bar deformation, the larger dowel could not take full advantage of the energy dissipation capacity. The volume loss ratio of wire meshes greater than or equal to 7.6 mm was measured as less than 3.5% regardless of the dowel bar

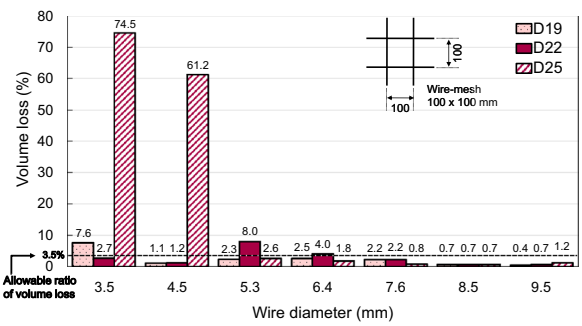

Fig. 5 Results of parametric study on varying dowel bar sizes and wire diameters

size. Among them, the combination of 7.6 mm wire mesh (100 mm × 100 mm) and 19 mm dowel bar could be the optimal and most economical design for the CMB-17S, as shown in Fig. 6. Details of the numerical results appear in the journal *Materials* (Lee et al., 2019). A full-scale field test of the proposed CMB-17S was also conducted in order that it could be installed along expressways (presented later in this paper).

2.3 Full-Scale Field Test of the CMB-17S

2.3.1 Test Conditions and Evaluation Criteria

A series of crash tests were conducted and evaluated, taking into account three areas: structural adequacy, occupant risk, and after-collision vehicle trajectory. In this study, the CMB-17S was designed to resist the SB6/H3 impact level or an IS of 420 kJ. According to the SB6 criteria in the crash test guidelines (MOLIT, 2015), a CMB must be subjected to full-scale field test conditions, including a 2500-kg truck impacting the safety barrier at 80 km/h and at a 15° angle, as shown in Fig. 7(a). In addition, occupant risk is appraised from the full-scale field test conditions, which involve a 1300-kg passenger car impacting the barrier at 100 km/h and at a 20° angle, as shown in Fig. 7(b).

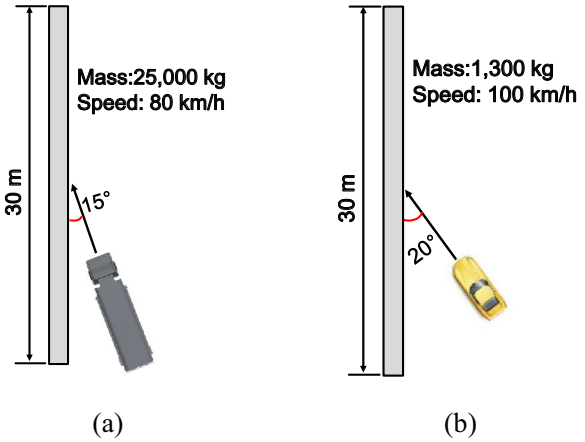

Fig. 7 Full-scale crash test conditions: (**a**) structural adequacy and (**b**) occupant risk

2.3.2 Preparation for the Full-Scale Field Test of CMB-17S

The CMB-17S installation consisted of a reinforced, permanent concrete barrier. The CMB-17S had to be constructed and installed to reflect the barriers currently in-service on the expressway and had to conform to the crash test guidelines. The barrier was 45 m long, 635 mm

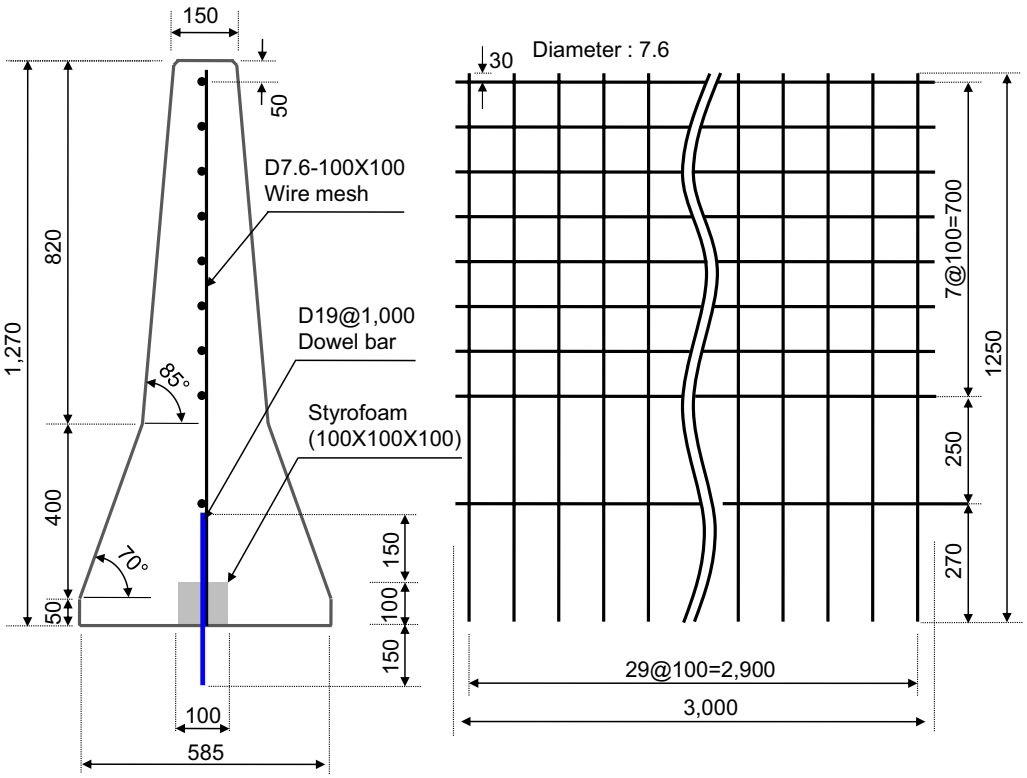

Fig. 6 Proposed design of the deformable concrete median barrier, CMB-17S (dimensions in millimeters)

wide at the base, and 150 mm wide at the top. The mean of the 28-day compressive strength of the concrete, based on 150 mm × 300 mm cylinders, was 31.2 MPa, whereas the specified concrete compressive strength was 30 MPa. The barrier reinforcement details are shown in Fig. 6. Before the slipforming operation, the wire mesh was aligned with the length of the CMB and the D19 dowel bars were installed at intervals of 1.0 m. More details regarding full-scale field testing preparation are in the journal *Materials* (Lee et al., 2019).

2.4 Crash Test Results

A full-scale vehicle crash test, using a 25,120-kg single unit truck at a speed of 81.5 km/h and at an impact angle of 15°, was performed on the CMB-17S and was deemed unacceptable according to structural adequacy criteria presented in the crash test guidelines. Fig 8 shows the concrete fragmentation caused by local impact between the lower corner of the steel cargo bed and the upper zone of CMB-17S. The concrete fragmentation violated the requirement regarding structural adequacy, because any barrier fragment greater than 2.0 kg should be no more than 2.0 m away from the barrier after collision (Fig. 8(b)).

3 Development of High-Performance Concrete Median Barrier, CMB-17F

3.1 Calibration of Vehicle-to-Barrier Model

The CMB-17S failed to meet performance criteria presented in the guidelines due to concrete fragmentation caused by local impact. When comparing the maximum lateral displacement between the full-scale field test and FE analysis, the full-scale field test results were 61% greater than those of the FE analysis. The FE model for a vehicle-to-barrier collision needs to be calibrated in order to reflect field test results. For this purpose, the frictional coefficient between the vehicle and barrier, and the curb weight (empty weight) of the vehicle were selected as key parameters (Lee et al., 2017). Lee et al. (2017) studied the effect of curb weight on load-time history caused by a vehicle–truck collision and it was found that a greater curb weight is associated with a greater impact load and impulse, when the total weight of the vehicle remains the same. A series of parametric studies were conducted on friction (0.5 and 0.6) and curb weight (7500, 8200, 9600, and 10,700 kg). Table 2 and Fig. 9 show results of the parametric study on various coefficients and curb weights in terms of volume loss ratio and maximum lateral displacement. The case of F0.5-W8.2 (friction coefficient of 0.5 and curb weight of 8200 kg) appears to be close to the full-scale field test. The lateral displacement was accurately estimated, and the volume loss ratio only differed by 2.0% from the full-scale field test results. Based on the results of the parametric study, the FE model of the vehicle-to-barrier collision was calibrated at 0.5 for the frictional coefficient and 8200 kg for the curb weight of the vehicle.

3.2 Development of Numerical Model for Local Failure

The CMB-17S with containment level SB6/H3, which was proposed based on the results of the parametric study conducted by Lee et al. (2019), did not satisfy the requirements specified by MOLIT (2015) owing to punching shear failure, which occurred at the second impact in the full-scale field test. Note that local punching shear failure was also observed during the vehicle-to-barrier collision on CMB-16 (IS = 456 kJ) (Lee et al., 2017). Additional numerical studies to analyze the local punching shear failure observed in full-scale field tests of CMB-17S (Lee et al., 2019) would be needed to evaluate the local impact energy. For this purpose, the impact conditions (i.e., mass, speed, or location) for the second impact of

Fig. 8 (**a**) Punching shear failure at top of the CMB-17S and (**b**) concrete fragmentation from the CMB-17S caused by punching shear failure

Table 2 Calibration of vehicle-to-barrier model

Type	Wire mesh size (mm)	Dowel bar size (mm)	Friction coefficient	Curb weight of vehicle (kg)	Ratio of vol. loss (%)	Max. lateral displacement (mm)
Full-scale field test of CMB-17S	7.6	19	–	13,350	8.7	50
Initial FE analysis of CMB-17S			0.8	7500	2.2	31
F0.5 – W8.2			0.5	8200	6.7	50
F0.5 – W9.6			0.5	9600	9.4	110
F0.5 – W10.7			0.5	10,700	4.9	166
F0.6 – W8.2			0.6	8200	5.1	41
F0.6 – W9.6			0.6	9600	5.7	40
F0.8 – W10.7			0.8	10,700	2.8	38

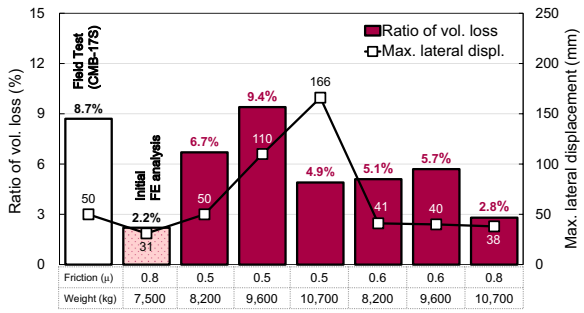

Fig. 9 Calibration of vehicle-to-barrier model by adjusting dynamic friction coefficient between vehicle and barrier, and curb weight of vehicle

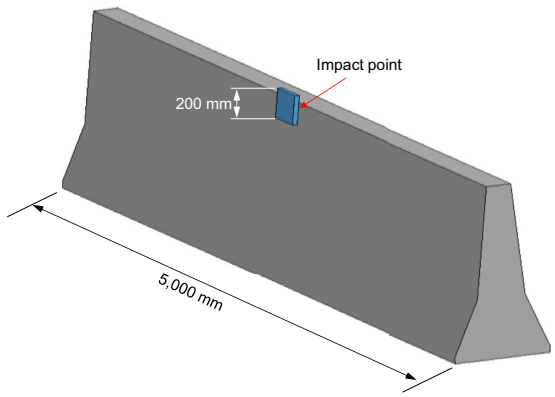

Fig. 10 Conceptual illustration of local failure model

both full-scale field tests were evaluated by video analysis. The impact speed and location of the second impact were found by video analysis from the full-scale field test of CMB-17S to be 20.7 km/h, at 1130 mm from the bottom. However, it was impossible to evaluate the impact mass at the second impact by visual analysis. Therefore, a numerically inverse analysis was conducted to assess the proper mass of the second impact. As shown in Fig. 10, a 200-mm rectangular steel plate with 30 mm thickness was used to model the local impact. The geometry of the steel plate was determined from the failure modes of the vehicles and CMB-17S. The CMB model length was 5000 mm, and the boundary condition between the foundation and CMB was assumed to be fixed. The lateral displacement measured at the second impact was negligible when compared with the third impact. For conservative design, the empty space at each dowel bar was excluded in this local model, for computational efficiency. The input values of the local model for the material model were the same as those in the vehicle–barrier collision model. The parametric study was conducted in order to evaluate the impact mass when comparing the punching failure modes at the second impact in the numerically developed local failure model with those in the full-scale field tests.

3.3 Verification of Developed Local Failure Model

The volume losses of the CMB-16 (IS = 456 kJ) (Kim et al., 2018) and CMB-17S (IS = 420 kJ) (Kim et al., 2019; Lee et al., 2019) under the local impact with various masses of the steel plate were predicted using the developed local model shown in Fig. 10. The obtained results were compared with the full-scale field test results, as shown in Fig. 11 (Kim et al., 2018, 2019; Lee et al., 2019). A comparison of the local model results with the full-scale field test results revealed that the local model could predict the local failure caused by the stress concentrations between the steel compartment of the truck and the upper part of the CMB. The damaged section of the CMB-16 and the punching shear failure of CMB-17S observed in both tests could be well predicted.

A sensitivity analysis of the steel plate mass to the amount of volume loss was conducted to evaluate the impact energy at the second impact during the full-scale field test of the heavy vehicle on the CMB-17S. Fig 12 compares the numerically obtained volume loss of the

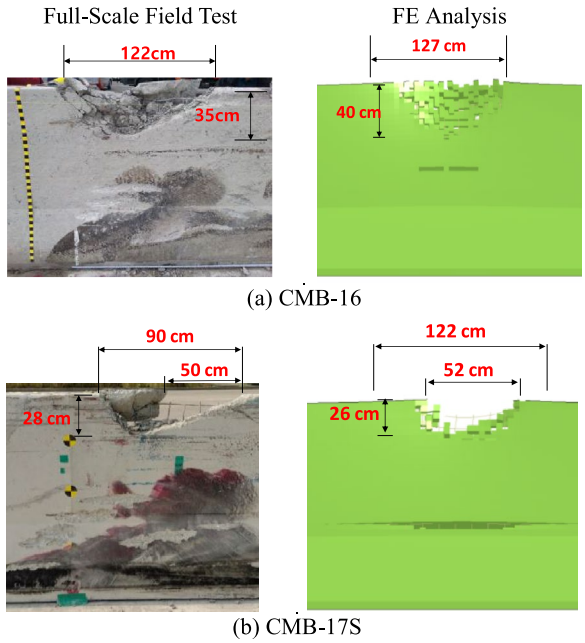

Fig. 11 Verification of local failure model by comparing failure modes between full-scale test and FE analysis

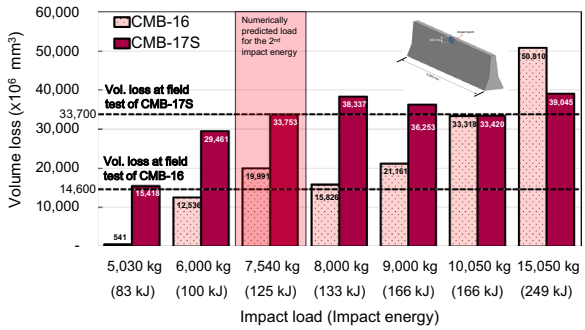

Fig. 12 Volume loss numerically evaluated against punching shear load

CMB-16 and -17S sections with various masses of steel plate. The steel plate mass 7540 kg (equivalent to 125 kJ of impact energy) showed similar results to the full-scale field test of the CMB-17S, based on results the sensitivity study. Although the mass increased beyond 7540 kg, no significant increase in volume loss of the CMB-17S appeared, as it reached an asymptotic limit between 8000 and 15,050 kg. This indicates that a mass of 7540 kg (about 30% of 25,000 kg) of the total mass of the truck was partially involved in local impact during the second impact. Therefore, the second impact energy of the full-scale field test on the CMB-17S could be estimated as 125 kJ, for a 7540-kg steel plate mass with a 20.7 km/h velocity (see Fig. 12). The numerical model for local failure with the 7540-kg steel plate mass and 20.7 km/h velocity was used to develop the CMB-17F, and determine whether it could withstand the second impact during the full-scale field test of the heavy vehicle.

3.4 Proposed High-Performance Concrete Median Barrier, CMB-17F

To improve CMB-17S (Lee et al., 2019) in this study, the width of the upper part was extended up to 50 mm to strengthen the upper part of the CMB-17S. This enlarged top width was first introduced in the CMB-16 to minimize concrete fragmentation and prevent poor concrete compaction of CMB during the slip-form construction (Lee et al., 2017). In addition, the wire mesh array was modified to strengthen the upper part of the CMB. As shown in Fig. 13, two D10 (10 mm diameter) horizontal wires were used at the top and the spacing between them varied from 75 to 100 mm. On the other hand, the spacing of the horizontal wire mesh at the lower part of the CMB was optimized to minimize the total reinforcement. This was done using a gradual decrease in spacing, such as 270, 250, 200, and 150 mm, as shown in Fig. 13. The spacing between the vertical steel reinforcements was set to 150 mm. Shock absorbers, which consisted of dowel bars and empty space, were also installed with the same spacing as those in the CMB-17S. The final design of the CMB-17F is shown in Fig. 13.

3.5 Numerical Evaluation of the Proposed CMB-17F

The proposed CMB-17F was numerically evaluated using the local failure model and the full vehicle-to-barrier collision model. Based on results from the sensitivity analysis of the steel plate mass to the amount of volume loss, the second impact energy of full-scale field test on the CMB-17S could be estimated as 125 kJ, for a 7540 kg steel plate mass with a 20.7 km/h velocity. The red box in Fig. 14 shows that the reduction in volume loss occurred under a punching shear energy that consisted of a 7540-kg steel plate mass and 20.7 km/h steel plate velocity. When compared with the volume loss of the CMB-17S under the same local impact conditions, that of the proposed CMB-17F was about 53% less than that of the CMB-17S.

The initial numerical model used to propose the CMB-17F was calibrated based on field test results of the CMB-17S. Fig 15 shows that the proposed CMB-17F was numerically evaluated using a calibrated numerical model of vehicle-to-barrier collision in terms of the volume loss ratio to maximum lateral displacement. The volume loss ratio of the CMB-17F was predicted within the allowable volume loss ratio and was 82% less than that of the CMB-17S. The maximum lateral displacement was

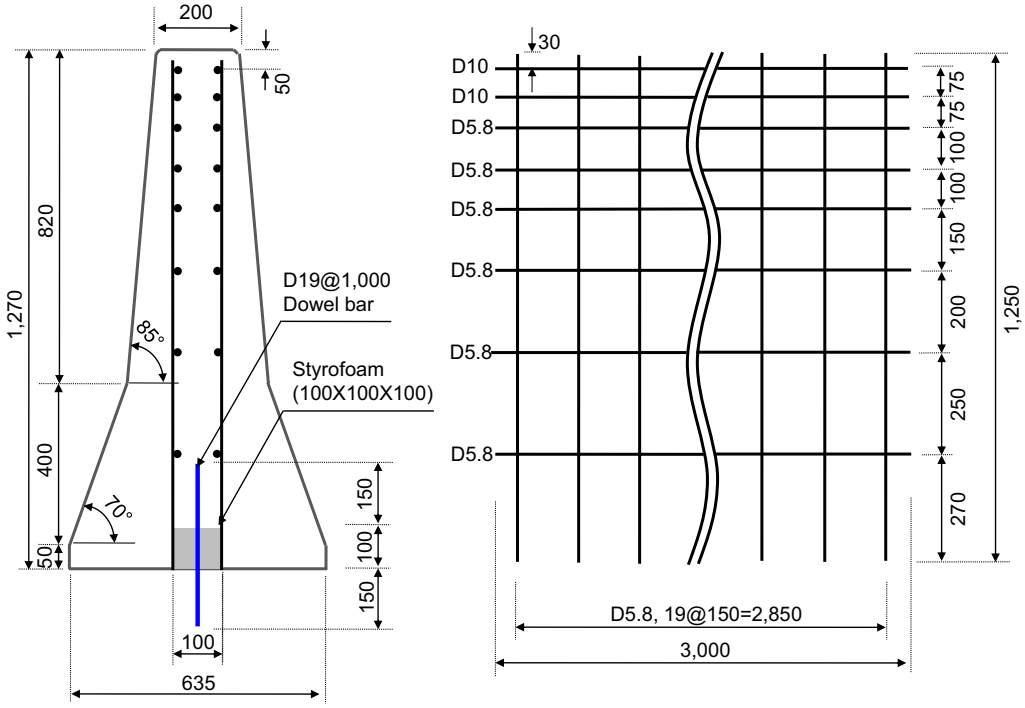

Fig. 13 Proposed design of high-performance concrete median barrier, CMB-17F (dimensions in millimeters)

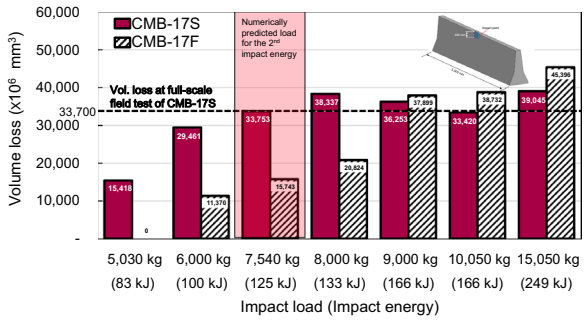

Fig. 14 Numerical evaluation of the proposed CMB-17F under punching shear load

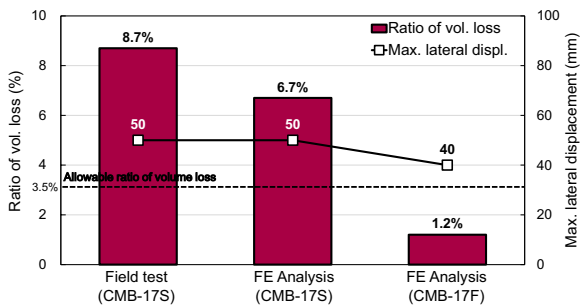

Fig. 15 Performance of the CMB-17F in terms of volume loss ratio and maximum lateral displacement in a vehicle-to-barrier collision

also estimated 40 mm, which appeared to be reasonable compared with the CMB-17S. Therefore, the proposed deformable CMB, CMB-17F was properly strengthened for the prevention of local failure and optimized for minimum total reinforcements based on results of numerical evaluation using the local failure model and the vehicle-to-barrier collision model.

4 Full-Scale Field Test of CMB-17F

The new CMB-17F was proposed based on a series of crash simulation data. To be accepted for use on the road, the new CMB must satisfy the requirements provided in the crash test guideline (MOLIT, 2015) specified by the transportation authority. A full-scale field test of CMB-17F was conducted and evaluated using the guideline for verification and validation of the crash simulation result.

4.1 Preparation for Full-Scale Field Tests of CMB-17F

The CMB-17F installation consisted of a reinforced, permanent concrete barrier, as shown in Fig. 16. The 45-m-long barrier was 635 and 200 mm wide at the base and at the top, respectively. The concrete used for the barrier had a 28-day concrete compressive strength of 36.1 MPa. The barrier reinforcement details are shown in Fig. 13. Before the slipforming operation, the wire meshes were aligned along the length of the CMB and the D19 dowel bars were installed at

Fig. 16 Installation of the proposed CMB-17F: Styrofoam allows for deformation and slipforming of the concrete median barrier

a spacing of 1.0 m for an intended deformation. The intended deformation under the impacts was allowed by a 100 mm × 100 mm × 100 mm Styrofoam cube placed under each dowel bar.

4.2 Full-Scale Test for Structural Adequacy

A 12.6-m cargo truck, shown in Fig. 17(a), was used to test for structural adequacy. The curb (empty) weight of the heavy vehicle was 13,530 kg. Ballast, which consisted of a cuboid-shape concrete mass, was placed on the middle of cargo bed to bring the total weight of the vehicle to 25,000 kg. Before the full-scale field test, 14 linear variable differential transformers (LVDT) were installed to measure the lateral displacement of CMB-17F during the crash test. To evaluate the body deformation of CMB-17F, four LVDTs (LVDT-1 … LVDT-4 in Fig. 17(b)) were mounted on steel frames, which were fixed to foundation slab. Other LVDTs (LVDT-5 … LVDT-14 in Fig. 17(b)) were placed 50 mm above the foundation slab at intervals of one or two meters to measure the resistance length of CMB-17F under the impact load. At impact, deformation signals were recorded at a sampling rate of 1,000 Hz.

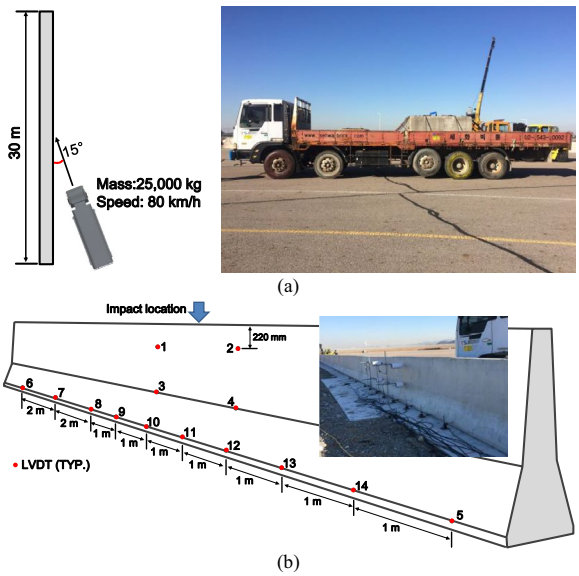

Fig. 17 Test setup: (**a**) test vehicle and (**b**) locations of the LVDTs

4.2.1 Results of Truck-To-Barrier Collision Test

The 25,070 kg loaded heavy vehicle hit the proposed CMB (CMB-17F) at a speed of 81.0 km/h and an angle of 15.0°, which resulted in an IS of 425.1 kJ. The measured impact conditions met containment level SB6/H3 (IS = 420 kJ), which is specified in the crash test guideline. At the time of the test, the truck was guided into the test installation using a remote controlled steering system. The truck impacted the barrier at 25 m from its upstream end. At 0.088 s, the lower-left-front corner of the truck contacted near the middle part of the barrier. At 0.292 s, the lower front bedside of the cargo truck contacted near the top of the barrier and test vehicle began to redirect. At 0.403 s, the truck began traveling parallel to the barrier. The test vehicle then continued along the barrier until it reached the end of the barrier wall. After impact, the vehicle exited the barrier and its trajectory did not violate the bounds of the exit box. The test vehicle subsequently came to rest 135 m downstream from its contact point with the concrete barrier. The CMB-17F received minor damage, with a small chip at its top.

Fig 18 shows the barrier displacements obtained from the LVDTs at impact. During the collision between the truck and barrier, three-step impact stages were significantly observed (Fig. 18). The same impact states were also observed and discussed by Kim et al. (2019) and

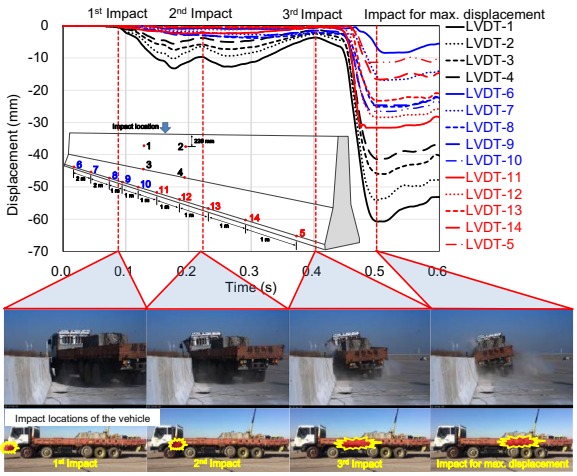

Fig. 18 Displacement of concrete median barrier under impacts

Lee et al. (2019). First, the left-front corner of the truck bumper zone contacted the barrier and then advanced continuously toward the barrier, which caused an increase in displacement without concrete fragmentation. The displacement kept increasing up to 13.2 mm, measured by LVDT-1 (solid black line in Fig. 18) until 0.176 s. Then, post-peak elastic recovery occurred before the second impact. Next, the lower-corner zone of the steel cargo bed collided with the upper zone of the barrier, increasing the displacement until 0.263 s, which was as much as the previous displacement induced by the first impact. The elastic deformation of the barrier recovered (the same increasing and decreasing slopes), and the deformation continued to recover until the third impact by the side compartment of the steel cargo bed, where the 11,720 kg concrete cuboid was located. At this impact stage, no concrete fragmentation was observed. Instead, about 60.7 mm of lateral displacement was measured by LVDT-1.

The lateral displacements of the barrier with respect to the longitudinal direction at different times are shown in Fig. 19. The measured displacements were 13.2 mm of the upper zone and 7.4 mm of the middle zone, whereas that of the bottom zone was less than 2.7 mm in the first impact (see the displacement at 0.176 s in Fig. 19). Given that the stiffness of CMB-17F was increased by extending the width of the top surface and adding more reinforcements at the top comparison with CMB-17S, the lateral displacements of the CMB-17F in the second impact appear to be less than 2.7 mm, measured by the bottom LVDTs, as much as those in the first impact. On the other hand, a residual displacement after the third impact was observed from all of the LVDTs that were installed to measure the bottom displacement of the barrier. The maximum permanent bottom displacement was 24.4 mm at the impact location, whereas the permanent displacement obtained from the first and last bottom LVDTs were 5.1 and 6.1 mm, respectively. Because permanent displacements were observed by all of the bottom LVDTs, the resistance length was determined to be more than 10 m. Fig 19 shows that the LVDT-measured displacements were very consistent with the lateral displacements obtained by surveys.

The resistance length was evaluated based on the permanent bottom displacements obtained by surveys. After the crash test, the permanent displacements at the bottom were measured every 1.0 m upstream and downstream with respect to the impact location. The maximum permanent displacement was 26.6 mm at the bottom. The permanent displacements were observed at 7.0 m downstream and 9.0 m upstream from the impact location, and then the resistance length of CMB-17F against containment level SB6/H3 (420 kJ) could be estimated as approximately 16.0 m, as shown in Fig. 20.

After the crash test, the barrier hardly sustained any noticeable damage except for some cosmetic damage in the form of tire marks on its front side. A few flexural cracks were observed on the back side of the barrier owing to vehicle impact loading. However, these were not penetrating cracks, which would lead to a decline in structural performance of the barrier. Nor was any concrete fragmentation found.

4.2.2 Comparison of Numerical and Experimental Results

Comparisons between the numerical and experimental results are shown in Fig. 21. It can be seen that discrepancies occurred in terms of the lateral displacements and the time of maximum lateral displacement. The maximum lateral bottom displacements at the impact location (LVDT-11) were observed as 31.6 mm for the full-scale field test and 25.4 mm for the numerical simulation, respectively, as shown in Fig. 21. This difference can be attributed to the mass distribution of the vehicle used in the field test and numerical simulation (see Fig. 22). For the vehicle used in the numerical simulation, the density of the cargo bed was increased in order to satisfy the vehicle mass condition of 25,000 kg (MOLIT, 2015). However, for the vehicle used in the full-scale field test, a 11,030-kg cuboid-shape concrete mass was placed on the middle of the cargo bed for ballast. Therefore, the mass concentration on the cargo bed during the full-scale field test led to an instantaneous high increase in impact energy, which

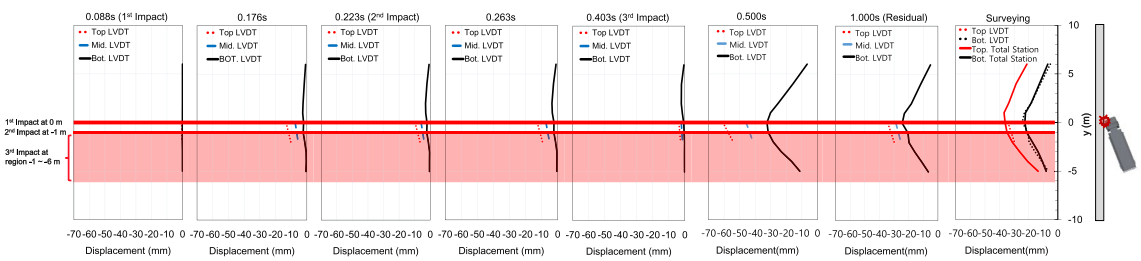

Fig. 19 Lateral displacement of the CMB-17F at different times

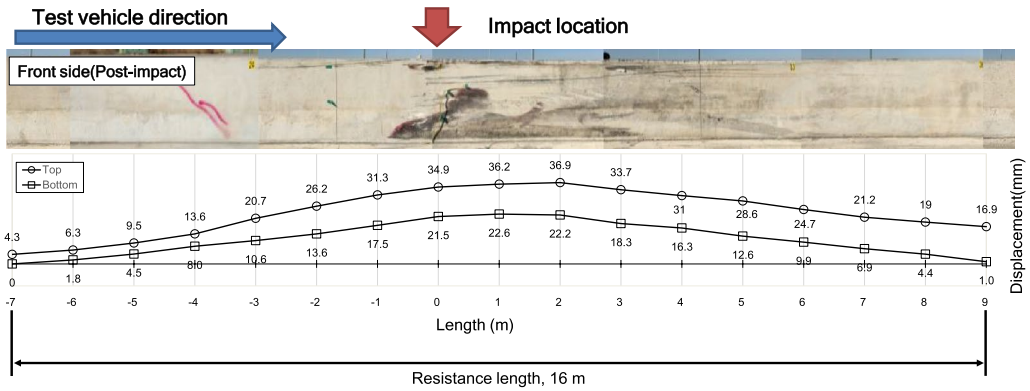

Fig. 20 Lateral displacement and resistance length of the CMB-17F

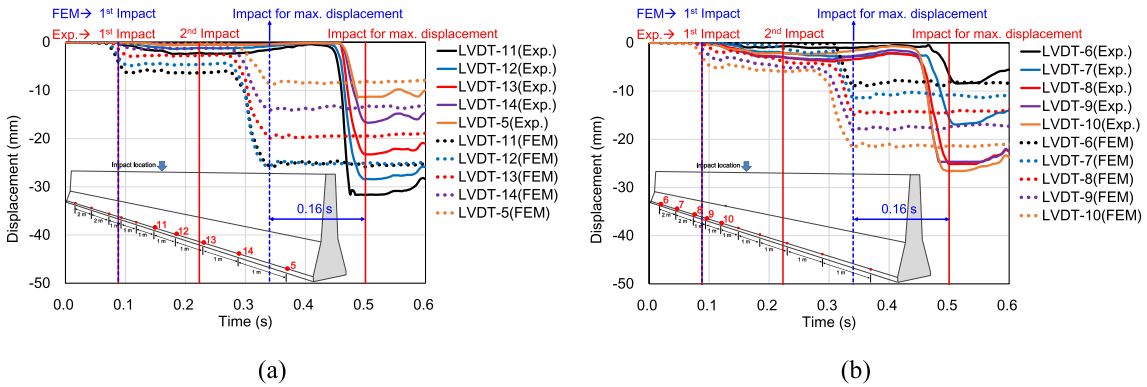

Fig. 21 (**a**) Comparison between numerical and experimental results: (**a**) bottom upstream and (**b**) bottom downstream with respect to impact location

induced a relatively larger maximum lateral displacement compared with the numerical simulation.

As for the time difference of the maximum lateral displacements between the full-scale field test and numerical simulation, it can be explained by the sizes of the vehicles used. The numerically obtained maximum lateral displacement occurred at the middle of the cargo bed, 4682 mm from the bumper, which impacted the barrier (see Fig. 22). However, it can be seen that the experimentally measured displacement occurred at 7854 mm from the bumper (see Fig. 22). Hence, it was numerically estimated that the maximum displacement occurred 0.16 s earlier when compared with that measured during the full-scale field test.

There are numerous complexities and uncertainties associated with numerical models and field tests, such as the choice of element types when designing the mesh, uncertainty in the geometric parameters of the model, uncertainty in the material property parameters of the chosen model, dynamic frictional coefficients between various materials, and uncertainty in the loading parameters of the model. The numerical model performed well and produced acceptable results in spite of complexities and uncertainties in the vehicle-to-CMB collision numerical model.

4.2.3 Comparison of CMB-17S and CMB-17F

After the crash test of CMB-17F, which was the strengthened version of CMB-17S (Lee et al., 2019) by adding more reinforcements to the upper part of the barrier and expanding its top width, the lateral displacement of CMB-17F could be compared with that of CMB-17S. Full-scale field tests of the two proposed barriers were conducted under the same test conditions (vehicle mass: 25,000 kg, vehicle speed: 80 km/h, and impact angle: 20°).

The experimental results for CMB-17F show three impacts observed at the same time, when the truck collided with CMB-17S (see Fig. 23). The first impact occurred at 0.088 s, the second impact occurred 0.135 s later, and then the last crash happened sequentially in 0.180 s. Each maximum lateral displacement with respect to the three impacts was measured at the same

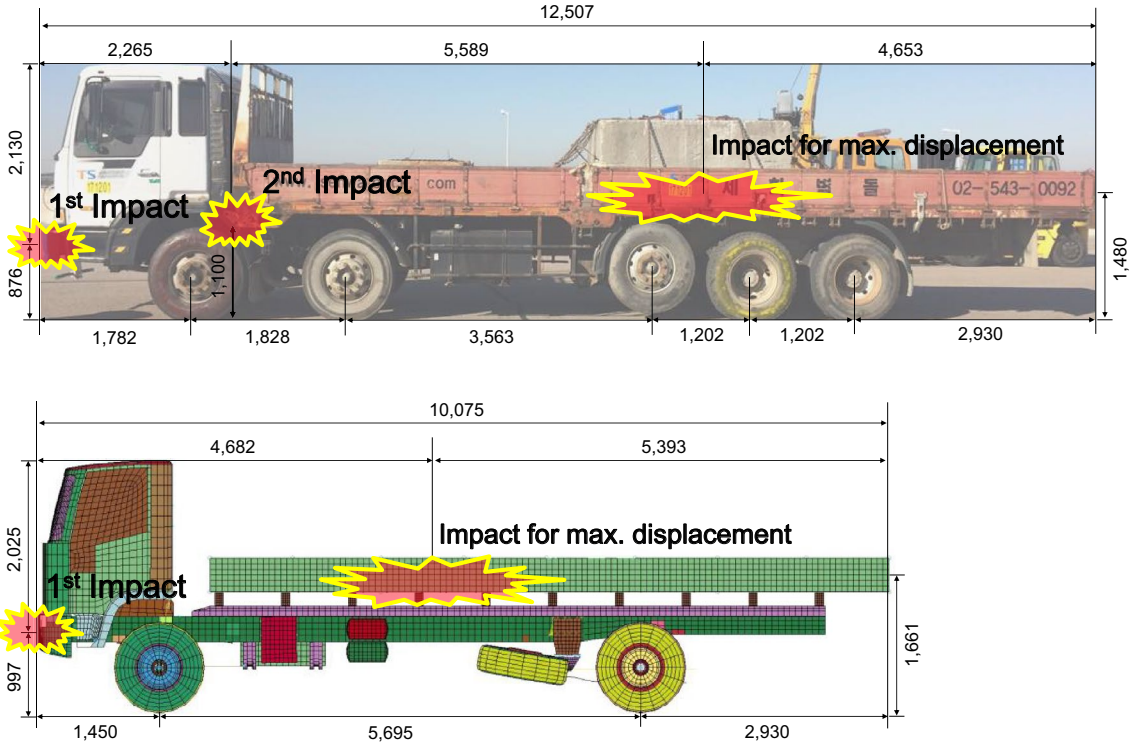

Fig. 22 Comparing vehicle impact locations to the CMB for full-scale field test (top) and numerical simulation (bottom) (dimensions in millimeters)

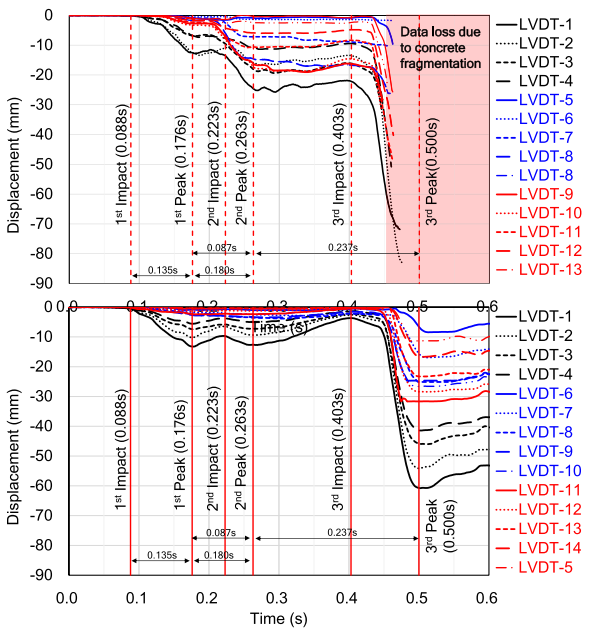

Fig. 23 Comparison of lateral displacements between CMB-17S (top) and CMB-17F (bottom)

time despite some time lag from the moment of impact. The lateral displacement of CMB-17F arose at the first impact of the left-front corner of the truck bumper zone, which resulted in a maximum displacement of 13.2 mm obtained from LVDT-1 (see Table 3). It should be noted that comparisons of the truck-to-barrier collisions between CMB-17S and CMB-17F were made using the lateral displacement data from LVDT-1 because they were the most distinct. While the truck kept pushing against the barrier after impact, the steel bumper started crushing with a decrease in lateral displacement. This implies that impact energy dissipated by the crushing of the bumper induced a decrease in the lateral displacement to 9.7 mm. Comparing ascending displacement rate with the descending one, with respect to the maximum displacement by the first impact, the absolute values of the rates seem to be very similar. This indicates that the CMB-17F behaved elastically when subjected to the first truck impact loading. On the other hand, the first impact on the CMB-17S barrier produced a similar maximum displacement (12.6 mm) to that of CMB-17F. However, the subsequent lateral displacements of CMB-17S increased continuously up to 24.6 mm without elastic recovery.

When it came to the second impact, CBM-17F generated as much displacement as the first impact and

Table 3 Lateral displacements obtained from LVDT-1 against three major impacts

	First impact	First peak	Second impact	Second peak	Third impact	Third peak
Time (*s*)	0.088	0.176	0.223	0.263	0.403	0.500
CMB-17S	0.0	12.6	11.5	24.6	22.2	≥ 71.8[a]
CMB-17F	0.0	13.2	9.7	12.8	3.7	60.7

[a] 71.8: this value was measured at 0.472 s because data measured from LVDT-1 prior to 0.472 s was not reliable due to concrete fragmentation

then its lateral displacement decreased until the third impact. In other words, it could be seen that CBM-17F exerted elastic recovery, maintaining its stiffness in spite of sequential impacts. However, CBM-17S was being pushed by the truck after the first impact and was additionally hit by the second impact, which led to a continuous increase in lateral displacement up to 24.6 mm. This was 95.2% higher than the first peak displacement caused by the first impact. Consequently, CBM-17S did not recover elastically but held its lateral displacement until the third impact.

The largest displacements of both the CMB-17S and CMB-17F barriers were observed at the third impact, which created the greatest impact energy during the full-scale field test. The maximum displacement of the CMB-17F by the third impact was 60.7 mm, which is 4.6 times higher compared with the first peak displacement induced by the first impact. The barrier yielded and produced the permanent displacement, followed by the third maximum displacement. However, the CMB-17S showed a sharp increase in the lateral displacement caused by the third impact and in concrete fragmentation on the upper part of the barrier. The lateral displacement measured by LVDT-1 became unreliable after it was struck by local-failure-induced fragmentation. The reliable measurements of LVDT-1 continued until 0.472 s, which corresponded to 71.8 mm of lateral displacement before the measurement was interrupted. Therefore, the maximum displacement could be estimated as larger than 71.8 mm.

The distinct behaviors for the same impact loading between the CMB-17F and CMB-17S stemmed from a difference in stiffness. The CMB-17F was strengthened by means of added reinforcement and a top width compared with CMB-17S, which had experienced local failure in its upper part. Because the top width of CMB-17F was expanded 50 mm more than CMB-17S, which resulted in increased stiffness, CBM-17F showed elastic recovery at the second impact. The local failure, which was shown as a type of punching shear failure, was prevented by adding more steel reinforcement. This helped to avoid the local failure and hold its stiffness until the third impact. As a result, the increased stiffness improved the impact resistance of the barrier, which reinforced the CMB-17F. Consequently, when the CMB-17F was subjected to impact loading it behaved satisfactorily without severe damage or violating the crash test guidelines.

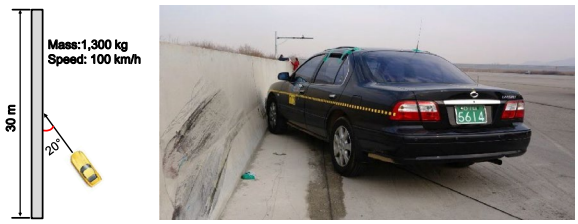

Fig. 24 Test setup for occupant risk

4.3 Full-Scale Test for Occupant Risk

In order to evaluate the proposed CMB (CMB-17F) for occupant risk, a Renault Samsung SM520 mid-size car, traveling at an impact speed of 100 km/h, impacted the CMB-17F, 30 m from the upstream end of the barrier installation. The left-front corner of the bumper struck the barrier at an impact angle of 20°, as shown in Fig. 24.

The 1325-kg vehicle hit the proposed CMB at a speed of 100.2 km/h and at an angle of 20°, which met the requirements specified in the crash test guideline. The bumper started to deform upon impact. At 0.168 s, the vehicle was traveling parallel to the barrier. At 0.438 s, the vehicle lost contact with the barrier. It did not penetrate or ride over the barrier, and it remained upright during and after the collision. Vehicle rolling and pitching, as shown in the summary, were considered acceptable in accordance with the guideline. After impact, the vehicle trajectory did not violate the bounds of the exit box.

Table 4 Results of full-scale test for occupant risk

	Measured value	Limit (MOLIT, 2015)
THIV (km/h)	30	33
PHD (g^a)	9	20
Rolling (°)	15.39	75
Pitching (°)	5.69	75

[a] *g* gravitational acceleration, 9.8 m/s^2

The barrier sustained only cosmetic damage, such as tire marks marked its front side. No cracks and no measurable deflections of the barrier were observed. The measured THIV and PHD values satisfied the specified limits of 33 km/h and 9 g, respectively, as shown in Table 4.

5 Conclusions

A high-performance CMB with a containment level of SB6/H3 (IS = 420 kJ) was proposed using a series of numerical simulations and full-scale field tests. In order to develop the high-performance CMB, the concept of a deformable CMB was introduced. This involved creating a small empty space under each dowel bar location so that the dowel bar could deform by bending under impact loading. The dowel bar, deformed by impact loading could successfully absorb a significant portion of the impact energy and disperse deformations within the resistance length, which dissipated the impact energy. Based on the impact simulations and crash tests, the following conclusions were drawn:

1. The deformable CMB, CMB-17F was finally proposed to contain an IS of SB6, which specifies a vehicle mass 25,000 kg, vehicle speed of 80 km/h, and impact angle of 20°.
2. The CMB-17F was designed with a 200-mm width of its upper part and two layers of wire mesh with different wire sizes and horizontal spacings to achieve both strengthening and optimization.
3. Based on the comparative analysis, CMB-17F is well optimized to reduce the total reinforcements and concrete in comparison with high-performance concrete median barriers due to a shock absorber.
4. The full-scale field test results of CMB-17F satisfied the impact safety standards in three appraisal areas: (1) structural adequacy, (2) occupant risk, and (3) vehicle trajectory after collision.
5. The proposed CMB-17F could reduce a large amount of concrete fragmentation at impacts compared with undeformable CMB with a containment level of SB5-B/H2 (IS = 270 kJ), which is currently installed on the expressway. In detail, the undeformable CMB produced a 7% volume loss at an IS of 270 kJ, whereas the CMB-17F rarely produced (volume loss of about 0.0%) despite harsher impact conditions such as an IS of 420 kJ.

Acknowledgements
The authors acknowledge the financial support of the Korea Expressway Corporation (KEC) and Basic Science Research Program through the National Research Foundation of Korea (NRF) funded by the Ministry of Education (2018R1D1A1B07049074).

Author contributions
YJ: formal analysis, field test, writing—original draft. IL: conceptualization, methodology. J.L.: investigation, writing—review and editing. KK: data curation, numerical simulation. GM: field test, data analysis. WK: methodology, writing—review and editing, project administration, funding acquisition. All authors read and approved the final manuscript.

Funding
This research was supported by the research fund of the Korea Expressway Corporation (KEC).

Availability of data and materials
All data generated or analyzed during this study are included in this published article.

Declarations

Competing interests
The authors declare that they have no competing interests.

Received: 30 January 2023 Accepted: 3 May 2023
Published online: 05 September 2023

References

AASHTO. (2016). Manual for assessing safety hardware (MASH). In. Washington, DC: Association of State Highway and Transportation Officials.
Ahn, H. I., Kim, D. S., Moon, B. K., & Kim, K. D. (2021). Assessment of structural adequacy of semi-rigid safety barriers. *International journal of crashworthiness*, 1–14.
Auyeung, S., Alipour, A., & Saini, D. (2019). Performance-based design of bridge piers under vehicle collision. *Engineering Structures, 191*, 752–765.
Borovinšek, M., Vesenjak, M., Ulbin, M., & Ren, Z. (2007). Simulation of crash tests for high containment levels of road safety barriers. *Engineering Failure Analysis, 14*(8), 1711–1718.
CEB-FIP. (2012). FIB Model Code for Concrete Structures 2010. In (pp. 434). New Jersey, U.S.: Ernst & Sohn publishing house.
CEN. (2012). EN 1317 European Standard for Road Restraint Systems. In.
Chung, C.-H., Lee, J.-W., Kim, S.-Y., & Lee, J.-H. (2011). Influencing factors on numerical simulation of crash between RC slab and soft projectile. *Journal of the Computational Structural Engineering Institute of Korea, 24*(6), 591–599.
Dinnella, N., Chiappone, S., & Guerrieri, M. (2020). The innovative "NDBA" concrete safety barrier able to withstand two subsequent TB81 crash tests. *Engineering Failure Analysis, 115*, 104660.
El-Tawil, S., Severino, E., & Fonseca, P. (2005). Vehicle collision with bridge piers. *Journal of Bridge Engineering, 10*(3), 345–353.
Ferdous, M. R., Abu-Odeh, A., Bligh, R. P., & Jones, H. L. (2013). Placement of traffic barriers on roadside and median slopes–guidelines based on numerical simulations. *International Journal of Crashworthiness, 18*(2), 110–125.
Ferdous, M. R., Abu-Odeh, A., Bligh, R. P., Jones, H. L., & Sheikh, N. M. (2011). Performance limit analysis for common roadside and median barriers using LS-DYNA. *International Journal of Crashworthiness, 16*(6), 691–706.
Grzebieta, R., Koay, K., & Zou, R. (1999). *Road-side crash barriers–Can they be modelled?* Paper presented at the Australian MADYMO Users Meeting
JRA. (2008). Installation specification of safety barrier and commentary. In. Tokyo, Japan: Japan Road Association
Kim, W., Lee, I., Jeong, Y., Zi, G., Kim, K., & Lee, J. (2018). Design approach for improving current concrete median barriers on highways in South Korea. *Journal of Performance of Constructed Facilities, 32*(3), 04018022.
Kim, W., Lee, I., Kim, K., Jeong, Y., & Lee, J. (2019). Evaluation of concrete barriers with novel shock absorbers subjected to impact loading. *Archives of Civil and Mechanical Engineering, 19*, 657–671.
Lee, J., Jeong, Y., Kim, K., Lee, I., & Kim, W. (2019). Experimental and numerical investigation of deformable concrete median barrier. *Materials, 12*(19), 1–21.
Lee, J., Zi, G., Lee, I., Jeong, Y., Kim, K., & Kim, W. (2017). Numerical simulation on concrete median barrier for reducing concrete fragment under harsh

impact loading of a 25-ton truck. *Journal of Engineering Materials and Technology, 139*(2), 021015.
LSTC. (2007). LS-DYNA Keyword user's manual volume I. In: livermore software technology corporation (LSTC).
Madurapperuma, M., & Niwa, K. (2014). *Concrete material models in LS-DYNA for impact analysis of reinforced concrete structures.* Paper presented at the Applied Mechanics and Materials.
MOLIT. (2015). Real Impact Test Guideline for Vehicle Safety Guard. In. Sejong, Korea: Ministry of Land, Infrastructure and Trasport.
Murray, Y. D. (2007). *Users manual for LS-DYNA concrete material model 159.* Retrieved from
Naish, D. A., & Burbridge, A. (2015). Occupant severity prediction from simulation of small car impact with various concrete barrier profiles. *International Journal of Crashworthiness, 20*(5), 510–523.
NCAC. (2020). National crash analysis Center. Retrieved from https://www.nhtsa.gov/crash-simulation-vehicle-models
Saini, D., & Shafei, B. (2018). Numerical investigation of CFRP-composite-strengthened RC bridge piers against vehicle collision. Retrieved from
Saini, D., & Shafei, B. (2019). Performance of concrete-filled steel tube bridge columns subjected to vehicle collision. *Journal of Bridge Engineering, 24*(8), 04019074.
Wu, Y., Crawford, J. E., & Magallanes, J. M. (2012). *Performance of LS-DYNA concrete constitutive models*. Paper presented at the 12th International LS-DYNA users conference
Yin, H., Fang, H., Wang, Q., & Wen, G. (2016). Design optimization of a MASH TL-3 concrete barrier using RBF-based metamodels and nonlinear finite element simulations. *Engineering Structures, 114*, 122–134.

Publisher's Note

Prof. Yoseok Jeong received Ph.D. degree in Civil Engineering from Pennsylvania State University, University Park, U.S.A. in 2012. Now he works at Department of Construction and Disaster Prevention Engineering, Kyungbuk National University, Sangjoo, Gyeongbuk, Republic of Korea. His research interest includes structural analysis.

Dr. Ilkeun Lee received Ph.D. degree in Civil Engineering from Hanyang University, Seoul, Republic of Korea in 2012. Now he works at Structure Research Division, Korea Expressway Corporation Research Institute, Hwaseong, Republic of Korea. His research interest includes design and maintenance of bridges.

Prof. Jaeha Lee received Ph.D. degree in Civil Engineering from Pennsylvania State University, University Park, U.S.A. in 2010. Now he works at Department of Civil Engineering, Korea Maritime & Ocean University, Busan, Republic of Korea. His research interest includes structural analysis and characterization of construction materials

Dr. Kyeongjin Kim received Ph.D. degree in Civil Engineering from Korea Maritime & Ocean University, Busan, Republic of Korea in 2021. Now he works at Department of Civil Engineering, Korea Maritime & Ocean University, Busan, Republic of Korea. His research interest includes structural analysis and structural reliability.

Geunhyeong Min is a Ph.D. student of Civil Engineering at Chungnam National University, Daejeon, Republic of Korea. His research interest includes structural analysis and concrete repair technologies for civil structures.

Prof. WooSeok Kim received Ph.D. degree in Civil Engineering from Pennsylvania State Universtiy, University Park, U.S.A. in 2008. Now he works at Civil Engineering Department of Chungnam National University, Daejeon, Republic of Korea. His research interest includes structural design and analysis and infrastructure maintenance.